catalysts

MDPI

Article

In Silico Switch from Second- to First-Row Transition Metals in Olefin Metathesis: From Ru to Fe and from Rh to Co

Jesús Antonio Luque-Urrutia, Martí Gimferrer, Èric Casals-Cruañas and Albert Poater *

Institut de Química Computacional i Catàlisi and Departament de Química, Universitat de Girona, Campus Montilivi, 17003 Girona, Spain; jesusantonio.luque@udg.edu (J.A.L.-U.); mgimferrer18@gmail.com (M.G.); eric.casals@hotmail.com (È.C.-C.)

* Correspondence: albert.poater@udg.edu; Tel.: +34-972-419403

Received: 20 November 2017; Accepted: 11 December 2017; Published: 14 December 2017

Abstract: Density functional theory (DFT) calculations have been used to investigate the behavior of different transition metals from Groups 8 (Fe and Ru) and 9 (Co and Rh) in an already well-known catalytic mechanism, which is based on an Ru(SIMes)(PPh_3)Cl_2=CH(Ph) complex. As expected, Ru has proven to perform better than their Fe, Co, and Rh counterparts. Even though the topographic steric maps analysis shows no difference in sterical hindrance for any of the metal centers, geometrically, the Fe-based species show a high rigidity with shorter and stronger bonds confirmed by Mayer Bond Orders. The systems bearing Co as a metallic center might present a reactivity that is, surprisingly, too high according to conceptual DFT, which would consequently be a drawback for the formation of the fundamental species of the reaction pathway: the metallacycle intermediate.

Keywords: cobalt; ruthenium; rhodium; density functional theory; olefin metathesis; iron; reaction mechanism; *N*-heterocyclic carbene; catalysis

1. Introduction

Olefin metathesis has been a widely studied reaction due to its particular use in diverse sectors, including relevant industrial applications such as the Shell Higher Olefin Process (SHOP) [1,2] and the Phillips Triolefin Process (PTP) [3] in petrochemistry and its use in polymerization reactions. Within homogeneous catalysis, the first catalysts for this process were developed by Grubbs [4,5] and Schrock [6]. This reaction consists of the reorganization of two carbon–carbon double bonds using a metal carbene complex as the catalyst, following Chauvin's [7,8] mechanism. The nature of the metal is fundamental, ruthenium and molybdenum being the leading metals for this research [9–11], with scarce studies on other metals, such as rhodium [12], osmium [13], and iron [14,15].

Since Ru- and Mo-based catalysts were first discovered by Grubbs and Schrock, respectively, due to the particular nature of the reaction, the need for new catalysts to deal with more specific reactions has increased. More catalysts are being continuously developed according to the amount of enantioselective synthesis required, the polymerization process as well as the construction of different polymers, and the opening or closure of rings where double bonds are involved [16–19]. Many of these chemical reactions are mainly based on ruthenium and other second-row transition metals, especially molybdenum, despite the remarkable performance also presented by tungsten and rhenium, from the third row. Even though the vast majority of catalysts are based on the metals mentioned above, there is a growing interest in promoting first-row transition metals for the sake of lower cost and toxicity [20,21], together with similar or slightly lower efficiency, leading to a low-cost generation of catalysts. Overall, the main problem in this sector is that, as the catalysis has increased in demand, so have the catalysts and their research. This is derived from the fact that the research involves less

abundant metals such as ruthenium, which results in high costs. Consequently, it has induced the need for catalysts based on cheaper and more abundant metals, such as the first-row transition metals, e.g., iron or cobalt [22], even though to date only in silico attempts have been found. This transition is required for the sustainability of the catalysts, which involves modern environment requirements, an optimization of the materials used and a reduction in toxic waste and costs [23] but, at the same time, improved efficiency [24–26]. As aforementioned, since experimental studies of these kinds of catalysts and their reactivity can be expensive, the use of computational tools has been gaining popularity in recent years [27,28]. In light of the experimental success of Ru-based catalysts with the SIMes *N*-heterocyclic carbene (SIMes = 1,3-bis(2,4,6-trimethylphenyl)-4,5-dihydroimidazole-2-ylidene), we wanted to expand our understanding of homologous Fe-based catalysts first computationally reported by Poater, Cavallo, et al. [14] and compare them with their Rh- and Co-based counterparts.

2. Results and Discussion

For the catalyst M(SIMes)Cl_2(=CHPh)PPh_3, where M = Ru, Rh, Fe, or Co, we illustrate its interaction with the essential olefin ethylene as a substrate in Scheme 1.

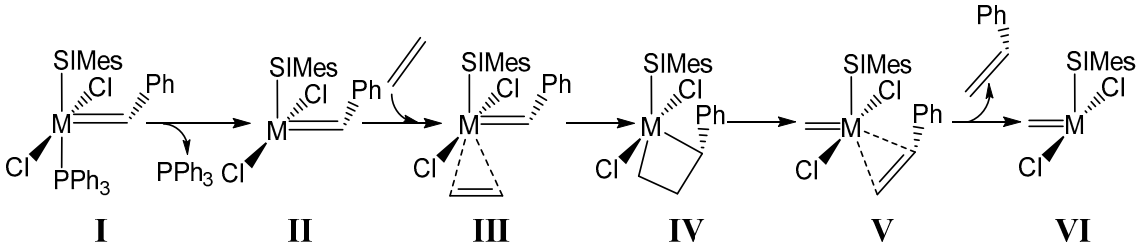

Scheme 1. Studied olefin metathesis reaction mechanism. M stands for the transition metal.

To unravel the olefin metathesis mechanism using a Co-based catalyst, we switched the Ru center by a cobalt atom in a known Grubbs olefin metathesis catalyst [29]. The latter consists of a ruthenium atom bonded to a SIMes-type ligand, two chlorides, a triphenylphosphine, and a phenylene group. Despite the apparent simplicity of the computational metal exchange, this leads to two problematic challenges. First, it entails switching from second to first row transition metals such as Co or Fe, which are prone to display high spin species, in agreement with Vasiliu et al. [30]. Consequently, this force screening the different multiplicity states for the first-row transition metal catalysts, not only for the first species **I** but through the whole reaction pathway. Second, ruthenium and iron, unlike cobalt and rhodium, bear an even number of electrons.

Based on past results with ruthenium [31], the potential energy surface was computed starting from the precatalyst **I** and using ethylene as substrate. The energy profile of the first cycle of the catalytic reaction, i.e., the activation of the catalyst, was calculated according to the mechanism described in Scheme 1. After the release of the labile phosphine ligand to form the 14e species **II**, the remaining steps are the coordination of the olefin (**III**), the metallacycle (**IV**), the generation of the second coordination intermediate (**V**) and finally, once the olefin is released, the second 14e species (**VI**). Having introduced the activation mechanism, before discussing the effectiveness depending on the metal center, the problem of the ground state for each metal and intermediate must be addressed. Differently from what happens for the first-row transition metals, ruthenium and rhodium as the ground state multiplicity only prefer the singlet and doublet states, respectively (see Table 1 and Table S3). Bearing the high qualitative similarity between the Gibbs free energies profiles in gas compared to the ones including the solvent correction with any of the exchange-correlation functionals used here, the next discussion is consistent with any methodology used for both first-row transition metal-based catalysts. Next, even though the energy profiles are nearly symmetrical for both second-row transition metals, differing by less than roughly 2–3 kcal/mol, the metallacycle

for rhodium is, incredibly, 15 kcal/mol more stable. Thus, the next opening of the four-membered ring becomes much more difficult, presenting a high energy barrier that hampers the feasibility of the Rh-based catalyst with respect to the Ru-based one, in accordance with the Mo-based Schrock catalysts [32,33].

Table 1. Computed stationary points (Gibbs free energies in kcal/mol) for the olefin metathesis reaction pathway for M(SIMes)Cl_2(=CHPh)PPh_3 (M = Ru and Rh) with ethylene as substrate (*m* = multiplicity; 1 = singlet; 2 = doublet; g = gas; s = solvent).

	Ru					Rh				
Method		**BP86-D3BJ/ TZVP**	**BP86-D3BJ/ TZVP**	**M06L/ TZVP**	**M06/ TZVP**		**BP86-D3BJ/ TZVP**	**BP86-D3BJ/ TZVP**	**M06L/ TZVP**	**M06/ TZVP**
	m	G_g	G_s	G_s	G_s	***m***	G_g	G_s	G_s	G_s
I	1	0.0	0.0	0.0	0.0	2	0.0	0.0	0.0	0.0
II	1	26.5	23.1	5.6	8.1	2	25.8	20.5	5.7	9.7
III	1	26.0	25.4	9.4	9.3	2	22.0	21.6	11.0	11.6
III–IV	1	30.7	30.7	15.4	13.5	2	29.2	28.2	19.9	21.0
IV	1	27.4	27.5	10.8	9.3	2	11.0	10.1	−3.9	−4.6
IV–V	1	34.2	33.3	17.6	15.3	2	36.3	34.7	24.0	24.2
V	1	32.2	31.8	16.1	14.1	2	32.4	31.5	20.0	18.6
VI	1	34.5	30.4	8.9	11.4	2	35.3	28.6	10.3	12.5

In Table 2, the activation mechanism in olefin metathesis for the series M(SIMes)Cl_2(=CHPh)PPh_3 (M = Fe and Co) is displayed (see Table S2). For these cobalt and iron structures, the complexity increases since both metals are prone to favor high spin multiplicities. Table 2 includes the energy values comparing their reaction pathways with different multiplicities to find out which is the ground state for each intermediate. It should be pointed out that, for some multiplicities, there are structures that cannot be located since some metal–carbon bonds break. The discussion on the solvent energy calculations is based on the BP86 functional [34–36] for the sake of consistency with the choice of multiplicity for each computed species, since the single-point energy calculations with the Truhlar functionals M06L [37] and M06 [38] may change the order of multiplicity, even though M06 was found to provide the right energy values for ruthenium as a metal center [39]. It is also important to point out that, for cobalt, the doublet state predominates, since the next quadruplet multiplicity is found to be from 10 to 20 kcal/mol higher in energy in all cases. Switching to iron, we can see a variety of multiplicities in the reaction mechanism ranging from singlet up to quintuplet, for the metallacycle **IV**, whereas triplet is the ground state of the other intermediates. Bearing the importance of the metallacycle in the olefin metathesis pathway [8,40], it is necessary to remark that for cobalt the metallacycle **IV** is not located since no multiplicity supports the four-membered ring, consequently breaking any of both Ru–C bonds.

Moving to the comparison between Fe-, Ru-, Co-, and Rh-based complexes, as shown in Tables 1 and 2 and summarized in Figure 1, it appears that, for Co and Fe, the first step that consists of the phosphine dissociation was more facile. This is promising since, for Ru, this is a drawback [41] and usually turns out to be the limiting step [42,43]. The energy cost is 23.1 kcal/mol for Ru but only 6.6 kcal/mol for Co. However, for the dissociative first step **I**→**II**, the trend is clear, favored by roughly 15 kcal/mol for both first-row transition metals [44]. Next, for the **II**→**III** step, only ruthenium and rhodium displayed a favorable coordination intermediate **III**, even if for Fe and Co this species is still achievable. Next, the central issue of the reaction pathway was found at Complex **IV** since for Co we were not able to locate the optimized geometry, which is the fundamental intermediate of the general reaction pathway described by Chauvin [7,8], leading us to think that this intermediate is not readily achievable for Co. We further tried to locate unsuccessfully a concerted transition state linking **III** directly with **V**, since all attempts to locate **IV** converged to either of these two coordination intermediates. As for the Fe-based complex, this metallacycle **IV** is very stable in agreement with

previous studies, which is a drawback in olefin metathesis. The latter fact, together with the quintuplet multiplicity of species **II** and **VI**, may be the main reasons for the limited effectiveness of iron as an olefin metathesis catalyst [45]. Indeed, the fact that, for the whole Ru-based reaction pathway, the singlet is the most stable spin state, together with its relatively unstable metallacycle **IV**, probably explains the experimental failure to obtain active Co- or Fe-based olefin metathesis catalysts.

Table 2. Computed stationary points (Gibbs free energies in kcal/mol) for the olefin metathesis reaction pathway for M(SIMes)Cl_2(=CHPh)PPh_3 (M = Fe and Co) with ethylene as substrate (*m* = multiplicity; 1 = singlet; 2 = doublet; 3 = triplet; 4 = quadruplet; 5 = quintuplet; 6 = sextuplet; g = gas; s = solvent) at the BP86-D3BJ/TZVP~sdd level of theory.

	Fe					Co				
Species	***m***	E_g	G_g	E_s	G_s	***m***	E_g	G_g	E_s	G_s
I	1	0.00	0.0	0.0	0.0	2	0.0	0.0	0.0	0.0
	3	5.1	3.1	4.1	2.0	4	11.4	11.7	13.8	14.2
	5	18.0	12.0	17.3	11.3	6	43.1	37.0	45.8	39.7
II	1	43.3	20.6	36.8	14.1	2	35.7	15.2	27.1	6.6
	3	38.4	17.5	29.3	8.4	4	44.1	26.9	36.1	18.9
	5	41.3	20.6	33.2	12.6					
III	1	34.0	31.2	30.0	27.2	2	32.9	29.2	29.6	25.9
	3	35.3	30.9	30.1	25.7					
	5	36.3	32.8	30.0	26.5	6	65.5	54.6	63.2	52.4
IV	1	26.5	25.4	23.2	22.1					
	3	18.0	11.4	14.8	8.2					
	5	3.5	−6.3	−2.6	−12.4					
	7	36.5	27.5	29.5	20.6					
V	1	26.3	23.8	22.6	20.1	2	37.9	32.8	35.9	30.8
	3	25.5	22.0	21.5	18.0					
	5	29.9	30.7	25.6	26.4	6	78.1	66.2	76.0	64.1
VI	1	55.5	32.0	48.2	24.6	2	53.9	31.7	45.0	22.8
	3	52.7	27.0	42.9	17.3	4	54.0	30.6	49.5	26.1
	5	58.0	31.0	48.8	21.8					

Geometrically, the facile phosphine dissociation cannot be explained directly by the elongation of the metal-P bond, as observed in Figure 2, but it requires the analyses of the latter bond using bond orders to take into account the different radius of each metal (see Table 3 and Table S1).

The structural data for the different molecules involved in the reaction mechanism for the four metals collected in Table 3 include the bonds between the respective metal and the nearby ligands. From the analysis of these data, we determined that, for Fe, the majority of the bonds are shorter; however, since the radius of the metals is fundamental to compare the strength of bonds bearing different metals, we further studied the Mayer Bond Orders (MBOs). It is possible to conclude that M–C and M=C bonds are stronger for Ru and Rh than for Fe and Co, respectively, in agreement with previous studies by Vasiliu et al. [30] and De Brito Sá et al. [45] related to the binding energy of the metal–carbene bond.

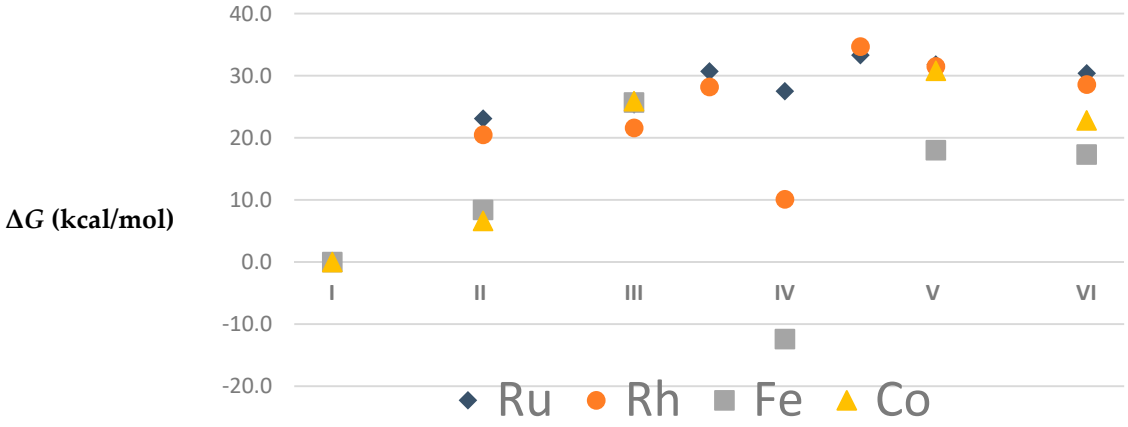

Figure 1. Reaction pathway (BP86-D3BJ/TZVP~sdd//BP86-D3BJ/TZVP~sdd Gibbs free energies in solvent in kcal/mol) for the olefin metathesis reaction pathway for M(SIMes)Cl_2(=CHPh)PPh_3 (M = Ru and Rh) with ethylene as substrate.

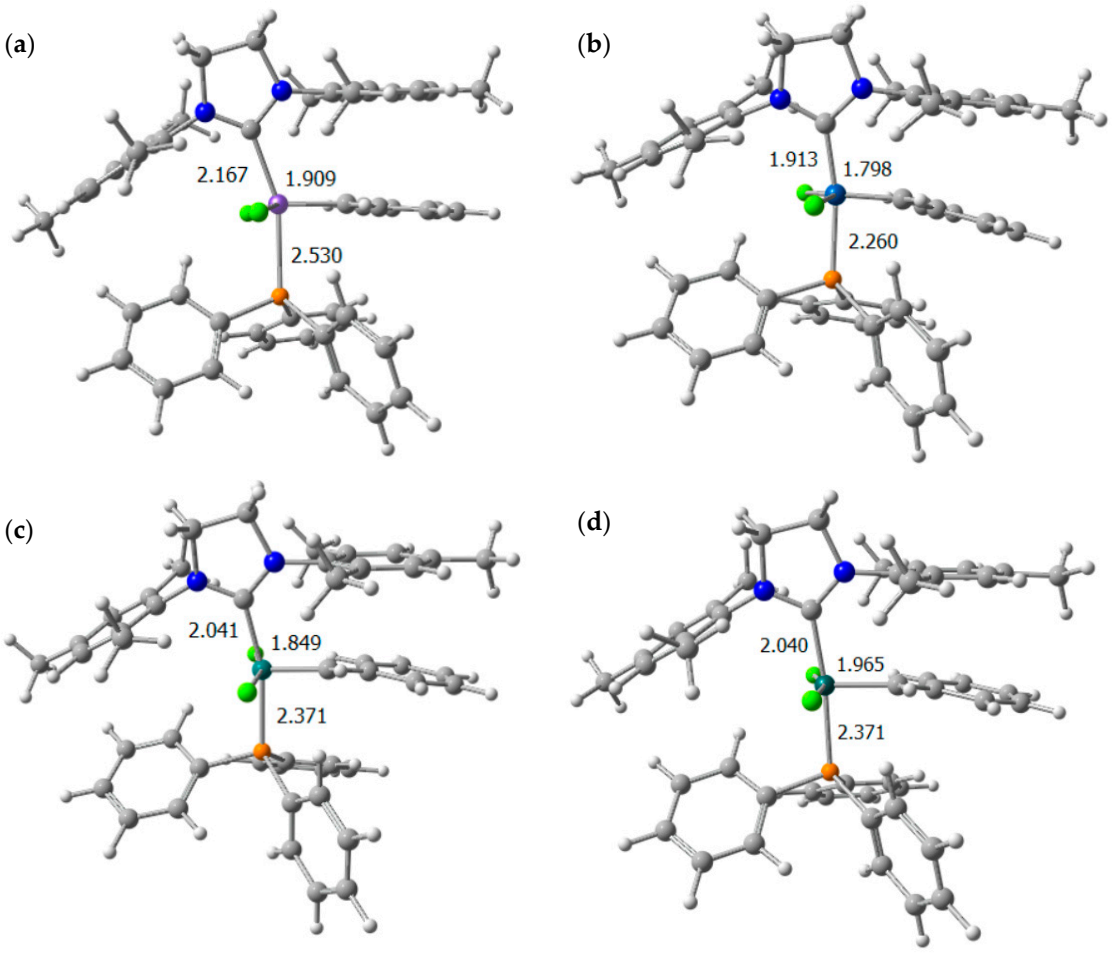

Figure 2. Computed structures for Complex **I** with (**a**) Fe; (**b**) Co; (**c**) Ru; and (**d**) Rh as the metal center. Selected distances are given in Å.

Table 3. Bond lengths (in Å) and Mayer Bond Orders (MBOs) for all the molecules involved in the mechanism for the Fe, Ru, Co, and Rh transition metals. (F = front and R = rear position of the chlorides according to the orientation in Figure 1, and the labeling Ru=C and Ru–C is maintained throughout the whole reaction pathway for the sake of clarity).

Fe			Ru			Co			Rh		
Bond		**Distance**	**MBO**		**Distance**	**MBO**		**Distance**	**MBO**		**Distance**	**MBO**
$M–C_{SIMes}$		1.931	0.94		2.041	0.93		1.913	0.92		2.040	0.83
M=C		1.747	1.74		1.849	1.75		1.798	1.44		1.965	1.01
M–Cl (F)	**I**	2.311	1.19	**I**	2.426	1.05	**I**	2.415	0.85	**I**	2.385	1.17
M–Cl (R)		2.285	1.05		2.422	0.91		2.352	0.92		2.364	0.89
M–P		2.272	0.99		2.371	0.84		2.260	0.97		2.371	0.90
$M–C_{SIMes}$		2.102	0.74		1.918	1.32		1.867	1.03		1.956	1.06
M=C	**II**	1.770	1.40	**II**	1.843	1.67	**II**	1.756	1.31	**II**	1.901	1.30
M–Cl (F)		2.205	1.36		2.316	1.03		2.184	1.26		2.360	0.92
M–Cl (R)		2.262	1.07		2.324	1.02		2.283	0.99		2.328	0.92
$M–C_{SIMes}$		1.922	0.97		1.994	1.02		1.892	0.93		2.004	0.87
M–C		2.306	0.48		2.304	0.46		2.169	0.50		2.283	0.48
M=C	**III**	1.753	1.67	**III**	1.870	1.62	**III**	1.869	1.10	**III**	1.993	0.97
M–Cl (F)		2.335	1.17		2.406	1.17		2.337	1.07		2.375	1.18
M–Cl (R)		2.311	1.12		2.410	1.02		2.338	1.00		2.370	1.03
$M–C_{SIMes}$		2.120	0.91		2.001	1.17					1.969	1.01
M–C		1.980	0.86		1.982	0.95					2.068	0.89
M=C	**IV**	2.067	0.74	**IV**	1.996	0.99	**IV**	Not located		**IV**	2.354	0.29
M–Cl (F)		2.246	1.20		2.408	0.92					2.375	1.05
M–Cl (R)		2.243	1.17		2.406	0.91					2.372	1.15
$M–C_{SIMes}$		1.914	1.06		2.031	0.92		1.925	0.73		1.997	0.87
M–C		1.725	1.89		1.826	1.77		1.743	1.76		1.962	1.08
M=C	**V**	2.284	0.45	**V**	2.282	0.47	**V**	2.493	0.17	**V**	2.353	0.39
M–Cl (F)		2.314	1.15		2.434	0.99		2.244	1.09		2.376	1.00
M–Cl (R)		2.295	1.11		2.428	1.06		2.246	1.08		2.391	1.10
$M–C_{SIMes}$		2.092	0.77		1.923	1.39		1.869	1.00		1.954	1.04
M–C	**VI**	1.722	1.80	**VI**	1.810	1.86	**VI**	1.716	1.78	**VI**	1.866	1.40
M–Cl (F)		2.227	1.14		2.318	0.90		2.260	0.99		2.342	0.92
M–Cl (R)		2.198	1.20		2.316	0.94		2.168	1.14		2.339	0.94

Bearing in mind that the olefin metathesis mechanism involves the coordination of a CH_2=CH_2 molecule to the metal center, which occurs between **II** and **III**, we performed an analysis of the accessibility for the metal center using the SambVca 2.0 web tool [46]. To view the occupied region close to the bonding distance of ethylene, we chose Complex **I**, without the phosphine, instead of **II**, since it better represents the real structure. In **II** (see the Supplementary Materials) [47], without the phosphine yet, the chloride atoms may alter the accessibility to the metal environment, rotating further from the SIMes ligand. Overall, it is evident from Figure 3 that, for the studied M-based complexes (M = Co, Fe, or Ru), all initial species **I** present sterics that are quite similar. Even though the bond distance with the ylidene moiety is shorter for Co and Fe than it is for Ru, neither the metal center with Co nor that with Fe are significantly more sterically congested than that with Ru, according to Figure 3. There are no vast differences at a glance [48,49]. Quantifying the percent buried volume (%VBur), we collected 46.0%, 46.1%, 46.2%, and 46.1% of buried volume for Fe, Co, Ru, and Rh, respectively. The data confirm that the metal site accessibility does not differ in any of the metals. Thus, we can exclude it from being a possible cause for the different performance of the three catalysts.

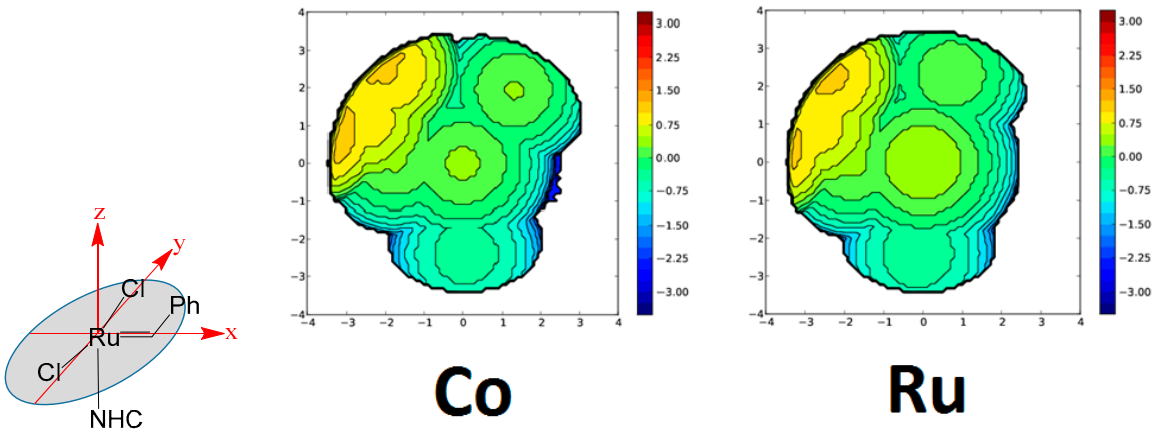

Figure 3. Topographic steric maps for the Co- and Ru-based catalyst **I**. The metal is at the origin, and the P atom is on the *z*-axis (Bz = benzylidene). The isocontour curves of the steric maps are given in Å. The radius of the sphere around the metal center was set to 3.5 Å; the Bondi radii were scaled by 1.17 for all the atoms, and a mesh of 0.1 Å was used to scan the sphere for buried voxels.

To round up all the obtained steric data, from an electronic point of view, we collected the data for the frontier molecular orbitals for each metal mechanism, and we used them for a conceptual DFT analysis. As shown in Table 4, Co-based complexes appear not to be exceptionally hard, which might induce to their non-existence, or at least to the difficulty in finding them due to their high reactivity. As for Ru and Fe, Ru appears to be a bit less reactive than Fe since it has a higher chemical hardness than the Fe-based catalysts. On the other hand, the higher electrophilicity of the Ru-based complex recognizes that it is more prone to react with nucleophiles such as olefins. In agreement with this hypothesis, the Natural Bond Orbital (NBO) charges confirm that the charge on the metal become much more negative on the metallacycle **IV** for Ru (−0.144) with respect to Fe (−0.025) and with Rh (−0.078) in between.

Table 4. Highest occupied molecular orbital (HOMO), lowest unoccupied molecular orbital (LUMO), chemical hardness (η), and electrophilicity (ω) for the computed stationary points for the olefin metathesis reaction pathway for M(SIMes)Cl_2(=CHPh)PPh_3 (M = Ru, Co, and Fe).

Complex	HOMO	LUMO	η	ω
Fe-**I**	−0.204	−0.091	0.113	0.096
Fe-**II**	−0.216	−0.104	0.112	0.114
Fe-**III**	−0.160	−0.119	0.041	0.237
Fe-**IV**	−0.158	−0.124	0.034	0.292
Fe-**V**	−0.165	−0.115	0.050	0.196
Fe-**VI**	−0.241	−0.114	0.127	0.124
Ru-**I**	−0.145	−0.099	0.046	0.162
Ru-**II**	−0.169	−0.105	0.064	0.147
Ru-**III**	−0.156	−0.112	0.044	0.204
Ru-**IV**	−0.154	−0.100	0.054	0.149
Ru-**V**	−0.158	−0.099	0.059	0.140
Ru-**VI**	−0.174	−0.094	0.080	0.112
Co-**I**	−0.137	−0.117	0.020	0.403
Co-**II**	−0.166	−0.126	0.040	0.266
Co-**III**	−0.141	−0.124	0.017	0.516
Co-**V**	−0.158	−0.121	0.037	0.263
Co-**VI**	−0.178	−0.123	0.055	0.206
Rh-**I**	−0.118	−0.098	0.021	0.282
Rh-**II**	−0.149	−0.128	0.021	0.456
Rh-**III**	−0.130	−0.109	0.021	0.343
Rh-**IV**	−0.160	−0.138	0.022	0.505
Rh-**V**	−0.134	−0.102	0.032	0.215
Rh-**VI**	−0.158	−0.127	0.031	0.326

3. Computational Details

All the DFT static calculations were performed with the Gaussian09 set of programs (Gaussian09.D01, Gaussian, Inc., Wallingford, CT, USA, 2009) [50]. The electronic configuration of the molecular systems was described with the triple zeta valence polarization function of Ahlrichs and co-workers for H, C, N, P, and Cl (TZVP keyword in Gaussian) [51]. Cobalt, iron, and ruthenium were described by the small-core, quasi-relativistic Stuttgart/Dresden effective core potential, with an associated valence basis set, contracted (standard SDD keywords in Gaussian09) [52–54]. The geometry optimizations were performed without symmetry constraints, and the characterization of the located stationary points was achieved by analytical frequency calculations, using the BP86 functional of Becke and Perdew [32–34], together with the Grimme D3BJ correction term to the electronic energy [55,56].

Single-point calculations of the BP86-D3BJ optimized geometries were performed using the BP86 [32–34], M06L and M06 functionals [37,38], and, were performed again with the triple-z basis set of Weigend and Ahlrichs for main-group atoms (TZVP keyword in Gaussian), whereas the SDD basis set was employed for ruthenium. Solvent effects were included with the polarizable continuous solvation model (PCM) using CH_2Cl_2 as solvent [57,58]. The reported free energies in this work include energies obtained at the M06/TZVP level of theory corrected with zero-point energies, thermal corrections, and entropy effects evaluated at 298 K.

%VBur Calculations: The buried volume calculations were performed with the SambVca package developed by Cavallo et al. [59]. The radius of the sphere around the origin placed 2 Å below the metal center was set to 3.5 Å, while for the atoms we adopted the Bondi radii scaled by 1.17, and a mesh of 0.1 Å was used to scan the sphere for buried voxels. The steric maps were evaluated with a development version of the SambVca package [46,60].

The electrophilicity of the complexes was evaluated as the Parr electrophilicity index (ω) calculated as $\omega = \mu^2/2\eta$, where μ and η are the chemical potential and the molecular hardness, respectively [61]. In the framework of DFT, μ and η for an N-electron system with total electronic energy E and subject

to an external potential are defined as the first and second derivatives of the energy concerning N at a fixed external potential. In numerical applications, μ and η are approximated with the finite difference formulas ($\mu = 0.5(\varepsilon_L + \varepsilon_H)$ and $\eta = 0.5(\varepsilon_L - \varepsilon_H)$), which are based on Koopmans' theorem. The ε_H and ε_L are the energies of the highest occupied molecular orbital (HOMO) and the lowest unoccupied molecular orbital (LUMO), respectively [62].

4. Conclusions

We have studied a well-known olefin metathesis mechanism with Ru, and that of homologous Rh, using two other abundant metals, Fe and Co. Rh, for the sake of complete comparison, was taken into account to cover the first two metal elements from Groups 8 and 9. Co-based catalyst turns out to be very reactive, but the location of the metallacycle **IV** is not feasible. Experimental research with this metal has not yet yielded any results, and here we argue a hypothesis. For Fe-based complexes, we have determined that Fe in fact presents stronger bonds than the Ru counterpart, even though, for the vital bond, which is the M=C bond, ruthenium bears stronger bonds. Analysis of the topographic steric maps data showed that, for all metals, the sterical hindrance is not an issue since they resemble each other, and therefore, there should not be sterical impediments for the entering olefin. On the other hand, electronically, Fe-based catalysts vary their ground state multiplicity throughout the mechanism, going from singlet up to quintuplet, which may be a drawback for their effectiveness, apart from the relatively exaggerated stability of its metallacycle, which is also partially a problem for the Rh-based counterpart. Chemical hardness analyses determined that Ru is more prone to react with a nucleophilic olefin than Fe-based catalysts. Still, ruthenium continues leading the list for new generations of olefin metathesis catalysts [63–65]. However, we have to keep going on the research to stabilize the metallacycle bearing Co as a metal center, which was the only drawback found for this metal in this study.

Supplementary Materials: The following are available online at www.mdpi.com/2073-4344/7/12/389/s1, Table S1: 3D view, *xyz* coordinate data sets and absolute energies (a.u.) for the DFT optimized molecular systems, Table S2: Computed stationary points (energies in kcal/mol) for the olefin metathesis reaction pathway for M(SIMes)Cl_2(=CHPh)PPh_3 (M = Fe and Co) with ethylene as a substrate (*m* = multiplicity; 1 = singlet, 2 = doublet, 3 = triplet, 4 = quadruplet, 5 = quintuplet, 6 = sextuplet; g = gas and s = solvent); Table S3: Computed stationary points (energies in kcal/mol) for the olefin metathesis reaction pathway for M(SIMes)Cl_2(=CHPh)PPh_3 (M = Ru and Rh) with ethylene as a substrate (*m* = multiplicity; 1 = singlet, 2 = doublet; g = gas and s = solvent).

Acknowledgments: A.P. thanks the Spanish MINECO for a project CTQ2014-59832-JIN and Xarxa de Química Teòrica i Computacional for a VALCHEM2016 project.

Author Contributions: A.P conceived and designed the calculations; all authors performed the calculations and analyzed the data; J.A.L.-U., M.G. and A.P. wrote the paper.

Conflicts of Interest: The authors declare no conflict of interest.

References

1. Lutz, E.F. Shell Higher Olefins Process. *J. Chem. Educ.* **1986**, *63*, 202–203. [CrossRef]
2. Reuben, B.; Wittcoff, H. The SHOP process an example of industrial creativity. *J. Chem. Educ.* **1988**, *65*, 605–607. [CrossRef]
3. Heckelsberg, L.F.; Banks, R.L.; Bailey, G.C. A tungsten oxide on silica catalyst for phillips triolefin process. *Ind. Eng. Chem. Prod. Res. Dev.* **1968**, *7*, 29–31. [CrossRef]
4. Rosebrugh, L.E.; Ahmed, T.S.; Marx, V.M.; Hartung, J.; Liu, P.; López, J.G.; Houk, K.N.; Grubbs, R.H. Probing stereoselectivity in ring-opening metathesis polymerization mediated by cyclometalated ruthenium-based catalysts: A combined experimental and computational study. *J. Am. Chem. Soc.* **2016**, *138*, 1394–1405. [CrossRef] [PubMed]
5. Scholl, M.; Ding, S.; Lee, C.W.; Grubbs, R.H. Synthesis and activity of a new generation of ruthenium-based olefin metathesis catalysts coordinated with 1,3-dimesityl-4,5-dihydroimidazol-2-ylidene ligands. *Org. Lett.* **1999**, *1*, 953–956. [CrossRef] [PubMed]

6. Schrock, R.R. Olefin metathesis by molybdenum imido alkylidene catalysts. *Tetrahedron* **1999**, *1999*, 8141–8153. [CrossRef]
7. Chauvin, Y. Olefin metathesis: The early days (Nobel Lecture 2005). *Adv. Synth. Catal.* **2007**, *349*, 27–33. [CrossRef]
8. Hérisson, J.L.; Chauvin, Y. Catalyse de transformation des olefins par les complexes du tungstène. *Makromol. Chem.* **1971**, *141*, 161–176. [CrossRef]
9. Bantreil, X.; Poater, A.; Urbina-Blanco, C.A.; Bidal, Y.D.; Falivene, L.; Randall, R.A.M.; Cavallo, L.; Slawin, A.M.Z.; Cazin, C.S.J. Synthesis and reactivity of ruthenium phosphite indenylidene complexes. *Organometallics* **2012**, *31*, 7415–7426. [CrossRef]
10. Rouen, M.; Queval, P.; Borré, E.; Falivene, L.; Poater, A.; Berthod, M.; Hugues, F.; Cavallo, L.; Baslé, O.; Olivier-Bourbigou, H.; et al. Selective metathesis of α-olefins from bio-sourced Fischer–Tropsch feeds. *ACS Catal.* **2016**, *6*, 7970–7976. [CrossRef]
11. Perfetto, A.; Costabile, C.; Longo, P.; Grisi, F. Ruthenium olefin metathesis catalysts with frozen NHC ligand conformations. *Organometallics* **2014**, *33*, 2747–2759. [CrossRef]
12. Poater, A. Moving from classical Ru-NHC to neutral or charged Rh-NHC based catalysts in olefin metathesis. *Molecules* **2016**, *21*, 177. [CrossRef] [PubMed]
13. Castarlenas, R.; Esteruelas, M.A.; Oñate, E. *N*-heterocyclic carbine-osmium complexes for olefin metathesis reactions. *Organometallics* **2005**, *24*, 4343–4346. [CrossRef]
14. Poater, A.; Vummaleti, S.V.C.; Pump, E.; Cavallo, L. Comparing Ru and Fe-catalyzed olefin metathesis. *Dalton Trans.* **2014**, *43*, 11216–11220. [CrossRef] [PubMed]
15. Poater, A.; Pump, E.; Vummaleti, S.V.C.; Cavallo, L. The activation mechanism of Fe-based olefin metathesis catalysts. *Chem. Phys. Lett.* **2014**, *610–611*, 29–32. [CrossRef]
16. Fürstner, A. Olefin metathesis and beyond. *Angew. Chem. Int. Ed.* **2000**, *39*, 3012–3043. [CrossRef]
17. Aeilts, A.L.; Cefalo, D.R.; Bonitatebus, P.J., Jr.; Houser, J.H.; Hoveyda, A.H.; Schrock, R.R. A readily available and user-friendly chiral catalyst for efficient enantioselective olefin metathesis. *Angew. Chem. Int. Ed.* **2001**, *113*, 1500–1504. [CrossRef]
18. Buchmeiser, M.R. Homogeneous metathesis polymerization by well-defined group VI and group VIII transition-metal alkylidenes: Fundamentals and applications in the preparation of advanced materials. *Chem. Rev.* **2000**, *100*, 1565–1604. [CrossRef] [PubMed]
19. Trnka, T.M.; Grubbs, R.H. The development of L_2X_2Ru=CHR olefin metathesis catalysts: An organometallic success story. *Acc. Chem. Res.* **2001**, *34*, 18–29. [CrossRef] [PubMed]
20. Poater, A.; Bahri-Laleh, N.; Cavallo, L. Rationalizing current strategies to protect *N*-heterocyclic carbene-based ruthenium catalysts active in olefin metathesis from C-H (de)activation. *Chem. Commun.* **2011**, *47*, 6674–6676. [CrossRef] [PubMed]
21. Poater, A.; Cavallo, L. A comprehensive study of olefin metathesis catalyzed by Ru-based catalysts. *Beilstein J. Org. Chem.* **2015**, *11*, 1767–1780. [CrossRef] [PubMed]
22. Goodall, B.L.; McIntosh, L.H., III; Rhodes, L.F. New catalysts for the polymerization of cyclic olefins. *Macromol. Symp.* **1995**, *89*, 421–432. [CrossRef]
23. Jorgensen, S.E. *Ecotoxicology and Chemistry Applications in Environmental Management*; CRC Press: London, UK, 2016.
24. Manzini, S.; Urbina-Blanco, C.A.; Poater, A.; Slawin, A.M.Z.; Cavallo, L.; Nolan, S.P. From Olefin Metathesis Catalyst to Alcohol Racemization Catalyst in One Step. *Angew. Chem. Int. Ed.* **2012**, *51*, 1042–1045. [CrossRef] [PubMed]
25. Pump, E.; Poater, A.; Zirngast, M.; Torvisco, A.; Fischer, R.; Cavallo, L.; Slugovc, C. Impact of electronic modification of the chelating benzylidene ligand in cis-dichloro configured 2nd generation Olefin Metathesis catalysts on their activity. *Organometallics* **2014**, *33*, 2806–2813. [CrossRef]
26. Manzini, S.; Poater, A.; Nelson, D.J.; Cavallo, L.; Slawin, A.M.Z.; Nolan, S.P. Insights into the decomposition of olefin metathesis pre-catalysts. *Angew. Chem. Int. Ed.* **2014**, *53*, 8995–8999. [CrossRef] [PubMed]
27. Du Toit, J.I.; van Sittert, C.G.C.E.; Vosloo, H.C.M. Metal carbenes in homogeneous alkene metathesis: Computational investigations. *J. Org. Chem.* **2013**, *738*, 76–91. [CrossRef]
28. Liu, P.; Xu, X.; Dong, X.; Keitz, B.K.; Herbert, M.B.; Grubbs, R.H.; Houk, K.N. Z-selectivity in olefin metathesis with chelated Ru catalysts: Computational studies of mechanism and selectivity. *J. Am. Chem. Soc.* **2012**, *134*, 1464–1467. [CrossRef] [PubMed]

29. Vougioukalakis, G.C.; Grubbs, R.H. Ruthenium-based heterocyclic carbene-coordinated olefin metathesis catalysts. *Chem. Rev.* **2010**, *110*, 1746–1787. [CrossRef] [PubMed]
30. Vasiliu, M.; Arduengo, A.J., III; Dixon, D.A. Role of electronegative substituents on the bond energies in the Grubbs metathesis catalysts for M = Fe, Ru, Os. *J. Phys. Chem. C* **2014**, *118*, 13563–13577. [CrossRef]
31. Poater, A.; Ragone, F.; Correa, A.; Cavallo, L. Comparison of different ruthenium–alkylidene bonds in the activation step with *N*-heterocyclic carbene Ru-catalysts for olefins metathesis. *Dalton Trans.* **2011**, *40*, 11066–11069. [CrossRef] [PubMed]
32. Poater, A.; Solans-Monfort, X.; Clot, E.; Copéret, C.; Eisenstein, O. DFT calculations of d0 M(NR)(CHtBu)(X)(Y) (M = Mo, W; R = CPh_3, 2,6-iPr–C_6H_3; X and Y = CH_2tBu, OtBu, OSi(OtBu)$_3$) olefin metathesis catalysts: Structural, spectroscopic and electronic properties. *Dalton Trans.* **2006**, 3077–3087. [CrossRef] [PubMed]
33. Poater, A.; Solans-Monfort, X.; Clot, E.; Copéret, C.; Eisenstein, O. Understanding d0-olefin metathesis catalysts: Which metal? Which ligands? *J. Am. Chem. Soc.* **2007**, *129*, 8207–8216. [CrossRef] [PubMed]
34. Becke, A. Density-functional exchange-energy approximation with correct asymptotic behaviour. *Phys. Rev. A* **1988**, *38*, 3098–3100. [CrossRef]
35. Perdew, J.P. Density-functional approximation for the correlation energy of the inhomogeneous electron gas. *Phys. Rev. B* **1986**, *33*, 8822–8824. [CrossRef]
36. Perdew, J.P. Erratum: Density-functional approximation for the correlation energy of the inhomogeneous electron gas. *Phys. Rev. B* **1986**, *34*, 7406. [CrossRef]
37. Zhao, Y.; Truhlar, D.G. A new local density functional for main-group thermochemistry, transition metal bonding, thermochemical kinetics, and noncovalent interactions. *J. Chem. Phys.* **2006**, *125*, 194101. [CrossRef] [PubMed]
38. Zhao, Y.; Truhlar, D.G. The M06 suite of density functionals for main group thermochemistry, thermochemical kinetics, noncovalent interactions, excited states, and transition elements: Two new functionals and systematic testing of four M06-class functionals and 12 other functionals. *Theor. Chem. Acc.* **2008**, *120*, 215–241.
39. Poater, A.; Pump, E.; Vummaleti, S.V.C.; Cavallo, L. The right computational recipe for olefin metathesis with Ru-based catalysts: The whole mechanism of ring-closing olefin metathesis. *J. Chem. Theory Comput.* **2014**, *10*, 4442–4448. [CrossRef] [PubMed]
40. Engel, J.; Smit, W.; Foscato, M.; Occhipinti, G.; Törnroos, K.W.; Jensen, V.R. Loss and reformation of ruthenium alkylidene: Connecting olefin metathesis, catalyst deactivation, regeneration, and isomerization. *J. Am. Chem. Soc.* **2017**, *139*, 16609–16619. [CrossRef] [PubMed]
41. Falivene, L.; Poater, A.; Cazin, C.S.J.; Slugovc, L.; Cavallo, L. Energetics of the ruthenium–halide bond in olefin metathesis (pre)catalysts. *Dalton Trans.* **2013**, *42*, 7312–7317. [CrossRef] [PubMed]
42. Urbina-Blanco, C.A.; Poater, A.; Lebl, T.; Manzini, S.; Slawin, A.M.Z.; Cavallo, L.; Nolan, S.P. The activation mechanism of Ru—Indenylidene complexes in olefin. *J. Am. Chem. Soc.* **2013**, *135*, 7073–7079. [CrossRef] [PubMed]
43. Leitgeb, A.; Abbas, M.; Fischer, R.C.; Poater, A.; Cavallo, L.; Slugovc, C. A latent ruthenium based olefin metathesis catalyst with a sterically demanding NHC ligand (pre)catalysts. *Catal. Sci. Technol.* **2012**, *2*, 1640–1643. [CrossRef]
44. Urbina-Blanco, C.A.; Leitgeb, A.; Slugovc, C.; Bantreil, X.; Clavier, H.; Slawin, A.M.Z.; Nolan, S.P. Olefin metathesis featuring ruthenium indenylidene complexes with a sterically demanding NHC ligand. *Chem. Eur. J.* **2011**, *17*, 5045–5053. [CrossRef] [PubMed]
45. De Brito Sá, E.; Rodríguez-Santiago, L.; Sodupe, M.; Solans-Monfort, X. Toward olefin metathesis with iron carbene complexes: Benefits of tridentate σ-donating ligands. *Organometallics* **2016**, *35*, 3914–3923. [CrossRef]
46. Falivene, L.; Credendino, R.; Poater, A.; Petta, A.; Serra, L.; Oliva, R.; Scarano, V.; Cavallo, L. SambVca 2. A web tool for analyzing catalytic pockets with topographic steric maps. *Organometallics* **2016**, *35*, 2286–2293. [CrossRef]
47. Poater, A.; Falivene, L.; Urbina-Blanco, C.A.; Manzini, S.; Nolan, S.P.; Cavallo, L. How does the addition of steric hindrance to a typical *N*-heterocyclic carbene ligand affect catalytic activity in olefin metathesis? *Dalton Trans.* **2013**, *42*, 7433–7439. [CrossRef] [PubMed]

48. Ahmed, S.M.; Poater, A.; Childers, M.I.; Widger, P.C.B.; LaPointe, A.M.; Lobkovsky, E.B.; Coates, G.W.; Cavallo, L. Enantioselective polymerization of epoxides using biaryl-linked bimetallic cobalt catalysts: A mechanistic study. *J. Am. Chem. Soc.* **2013**, *135*, 18901–18911. [CrossRef] [PubMed]
49. Poater, A.; Cavallo, L. Comparing families of olefin polymerization precatalysts using the percentage of buried volume. *Dalton Trans.* **2009**, *2009*, 8878–8883. [CrossRef] [PubMed]
50. Frisch, M.J.; Trucks, G.W.; Schlegel, H.B.; Scuseria, G.E.; Robb, M.A.; Cheeseman, J.R.; Scalmani, G.; Barone, V.; Petersson, G.A.; Nakatsuji, H.; et al. *Gaussian 09*; Gaussian Inc.: Wallingford, CT, USA, 2009.
51. Schäfer, A.; Huber, C.; Ahlrichs, R. Fully optimized contracted Gaussian basis sets of triple zeta valence quality for atoms Li to Kr. *J. Chem. Phys.* **1994**, *100*, 5829. [CrossRef]
52. Haeusermann, U.; Dolg, M.; Stoll, H.; Preuss, H. Accuracy of energy-adjusted quasirelativistic ab initio pseudopotentials. *Mol. Phys.* **1993**, *78*, 1211–1224. [CrossRef]
53. Kuechle, W.; Dolg, M.; Stoll, H.; Preuss, H. Energy-adjusted pseudopotentials for the actinides. Parameter sets and test calculations for thorium and thorium monoxide. *J. Chem. Phys.* **1994**, *100*, 7535–7542. [CrossRef]
54. Leininger, T.; Nicklass, A.; Stoll, H.; Dolg, M.; Schwerdtfeger, P. The accuracy of the pseudopotential approximation. II. A comparison of various core sizes for indium pseudopotentials in calculations for spectroscopic constants of InH, InF, and InCl. *J. Chem. Phys.* **1996**, *105*, 1052–1059. [CrossRef]
55. Grimme, S.; Antony, J.; Ehrlich, S.; Krieg, H. A consistent and accurate ab initio parametrization of density functional dispersion correction (DFT-D) for the 94 elements H-Pu. *J. Chem. Phys.* **2010**, *132*, 154104. [CrossRef] [PubMed]
56. Grimme, S.; Ehrlich, S.; Goerigk, L. Effect of the damping function in dispersion corrected density functional theory. *J. Comp. Chem.* **2011**, *32*, 1456–1465. [CrossRef] [PubMed]
57. Barone, V.; Cossi, M. Quantum calculation of molecular energies and energy gradients in solution by a conductor solvent model. *J. Phys. Chem. A* **1988**, *102*, 1995–2001. [CrossRef]
58. Tomasi, J.; Persico, M. Molecular interactions in solution: An overview of methods based on continuous distributions of the solvent. *Chem. Rev.* **1994**, *94*, 2027–2094. [CrossRef]
59. Poater, A.; Cosenza, B.; Correa, A.; Giudice, S.; Ragone, F.; Scarano, V.; Cavallo, L. SambVca: A web application for the calculation of buried volumes of *N*-heterocyclic carbene ligands. *Eur. J. Inorg. Chem.* **2009**, *2009*, 1759–1766. [CrossRef]
60. Jacobsen, H.; Correa, C.; Poater, A.; Costabile, C.; Cavallo, L. Understanding the M (SIMes) (SIMes = *N*-heterocyclic carbene) bond. *Coord. Chem. Rev.* **2009**, *253*, 687–703. [CrossRef]
61. Parr, R.G.; von Szentpaly, L.; Liu, S. Electrophilicity index. *J. Am. Chem. Soc.* **1999**, *121*, 1922–1924. [CrossRef]
62. Poater, A.; Gallegos, A.; Carbó-Dorca, R.; Poater, J.; Solà, M.; Cavallo, L.; Worth, A.P. Modelling the structure-property relationships of nanoneedles: A journey towards nanomedicine. *J. Comput. Chem.* **2009**, *30*, 275–284. [CrossRef] [PubMed]
63. Poater, A.; Credendino, R.; Slugovc, C.; Cavallo, L. Exploring new generations of ruthenium olefin metathesis catalysts: The reactivity of a bis-ylidene ruthenium complex by DFT. *Dalton Trans.* **2013**, *42*, 7271–7275. [CrossRef] [PubMed]
64. Martínez, J.P.; Vummaleti, S.V.C.; Falivene, L.; Nolan, S.P.; Cavallo, L.; Solà, M.; Poater, A. In silico olefin metathesis with Ru-based catalysts containing *N*-heterocyclic carbenes bearing C60 fullerenes. *Chem. Eur. J.* **2016**, *22*, 6617–6623. [CrossRef] [PubMed]
65. Wappel, J.; Fischer, R.C.; Cavallo, L.; Slugovc, C.; Poater, A. Simple activation by acid of latent Ru-NHC-based metathesis initiators bearing 8-quinolinolate co-ligands. *Beilstein J. Org. Chem.* **2016**, *12*, 154–165. [CrossRef] [PubMed]